JOURNAL OF COMPUTATIONAL PHYSICS 86, 294–313 (1990)

Interaction of Oscillating Filaments: A Computational Study

LISA J. FAUCI*

Department of Mathematics, Tulane University, New Orleans, Louisiana 70118

Received September 30, 1988; revised March 10, 1989

The immersed boundary technique is used to model the interaction of swimming filaments in a viscous, incompressible fluid. Fluid quantities are represented on a grid, and the immersed filaments are each represented by a discrete collection of moving points. The effects of phase differences and proximity of the filaments on energy dissipation and swimming speeds are studied. The computed results are compared with previous asymptotic analysis. Furthermore, we present case studies which exhibit phase-(un)locking phenomena undetectable using previous asymptotic analysis. © 1990 Academic Press, Inc.

1. INTRODUCTION

The principal means of swimming of aquatic animals is to pass waves of lateral displacement down the body. This type of propulsive motion spans the whole spectrum of Reynolds numbers, a nondimensional quantity which describes the ratio of inertial forces to viscous forces in the induced flow. For instance, the Reynolds number of a swimming eel is about 10^4, the nematode's about 1, and that of a spermatozoa about 10^{-3} [8].

It has been observed that when spermatozoa swim close together they tend to beat in synchrony [1]. When fish swim in schools it is also noticed that there are regular patterns of motion [2]. Ciliated organisms exhibit metachronal waves; cilia close together beat in synchrony, but there is a continuous phase difference along the surface [3]. One possible explanation for this type of coordinated motion is that "information" is transmitted by the fluid between the waving filaments.

In [4] we described a computational model of this undulatory mode of locomotion which was based upon the immersed boundary technique of Peskin [5]. There we analyzed a single oscillating, massless filament immersed in a two-dimensional fluid. We studied how dissipation of energy and overall swimming speed depended upon many parameters, including the Reynolds number and the wavelength, amplitude, and frequency of undulation.

* The author was supported in part by the National Science Foundation under Grant DMS-8 700858. All computing was done at the Pittsburgh Supercomputing Center.

0021-9991/90 $3.00

Due to the special way in which this computational model represents the immersed boundary, it is possible to study the swimming motion of more than one organism in the same domain of fluid. The effects of phase differences and proximity of oscillating filaments can be measured.

The swimming of neutrally buoyant organisms immersed in a viscous, incompressible fluid constitutes a coupled mechanical system. The state of the system at any time t is determined by the fluid velocity field $\mathbf{u}(\mathbf{x}, t)$ and the positions of the material points of the organisms $\mathbf{X}(s, t, l)$, where s is an arclength parameter and l denotes the particular organism.

The fluid is governed by the incompressible Navier–Stokes equation:

$$\rho\left(\frac{\partial \mathbf{u}}{\partial t}+\mathbf{u}\cdot\nabla\mathbf{u}\right)=-\nabla p+\mu\Delta\mathbf{u}+\mathbf{F}(\mathbf{x}, t)$$

$$\nabla\cdot\mathbf{u}=0.$$

Here ρ = density, μ = viscosity, $\mathbf{u}$ = velocity, and p = pressure.

The first equation is Newton's second law: mass density $\times$ acceleration = force density. The second states that the fluid is incompressible. The forces which appear are those due to pressure, viscosity, and the external force $\mathbf{F}(\mathbf{x}, t)$. The external force is used to represent the force of the organisms on the fluid. It is a delta function layer of force supported only by the regions of fluid which coincide with material points of an organism; away from these points the external force is zero. Since an organism is considered elastic and massless, the strength of the delta function force layer is determined at each instant by the local configuration of the organism. Representing the immersed swimming organisms as a singular force field in the fluid domain is the basis of the computational model.

The boundary conditions to be satisfied at the surfaces $\mathbf{X}(s, t, l)$ defined by the organisms are

$$\frac{d}{dt}\mathbf{X}(s, t, l)=\mathbf{u}(\mathbf{X}(s, t, l), t).$$

This states that the velocity of a point on an organism must be the same as the fluid velocity at that point.

The solution of this highly nonlinear coupled system is achieved computationally as described in [4]. In this paper we will briefly outline the computational scheme (Section 2). We will compare our results with the asymptotic analysis of G. I. Taylor [1] for zero Reynolds number flow (Section 3). Finally we will present the results of case studies which exhibit phenomena undetectable using previous asymptotic analysis.

2. Computational Model

We cover our two-dimensional fluid domain with a square grid on which we define the fluid quantities $\mathbf{u}_{ij}^n=\mathbf{u}(i\Delta x, j\Delta x, n\Delta t)$, p_{ij}^n and $\mathbf{F}_{ij}^n$. In contrast to this

Eulerian description of fluid quantities, the immersed organisms are modeled by collections of moving points $\mathbf{X}_{k,l}^n$, $l = 1, 2, 3, ..., nb$, where nb is the number of organisms within the domain and $k = 1, 2, 3, ..., m(nb)$, where $m(l)$ is the number of discrete points comprising organism l. These Lagrangian points do not coincide with grid points. The state of the system at time $t = n\Delta t$ is determined by $\mathbf{u}_{ij}^n$ and $\mathbf{X}_{k,l}^n$. From these, we need to advance another time step to determine $\mathbf{u}_{ij}^{n+1}$ and $\mathbf{X}_{k,l}^{n+1}$.

As explained in [4, 5], the coupling between fluid and boundary quantities occurs in two ways:

(1) The spreading of the force density $\mathbf{f}(s, t, l)$ defined on the immersed boundaries to the grid to determine the external force field $\mathbf{F}(x, t)$,

$$\mathbf{F}(\mathbf{x}, t) = \sum_{l=1}^{nb} \int_{B_l} f(s, t, l)\, \delta(\mathbf{x} - \mathbf{X}(s, t, l))\, ds.$$

(2) The interpolation of the fluid velocity $\mathbf{u}(\mathbf{x}, t)$ to material points in order to satisfy the no-slip condition

$$\frac{\partial \mathbf{X}}{\partial t} = \mathbf{u}(\mathbf{X}(s, t, l), t) = \int_{\Omega} \mathbf{u}(\mathbf{x}, t)\, \delta(\mathbf{x} - \mathbf{X}(s, t, l))\, d\mathbf{x}$$

for $l = 1, 2, 3, ..., nb$. (Note that δ is the two-dimensional delta function.)

These integral are discretized as sums,

$$\mathbf{F}_{ij}^n = \sum_{l=1}^{nb} \sum_{k} \mathbf{f}_{kl}^n D_{ij}(\mathbf{X}_{k,l})\, \Delta s$$

$$\mathbf{U}_{k,l}^n = \sum_{ij} \mathbf{u}_{ij}^n D_{ij}(\mathbf{X}_{k,l})\, \Delta x^2, \qquad l = 1, 2, ..., nb,$$

where D_{ij} is the discrete approximation to the two-dimensional delta function introduced by Peskin [5].

Since the immersed organisms are elastic and massless, the force densities are determined by the boundary configurations at time t. We want to specify a force density which will allow us to impose (approximately) a given swimming motion. This motion will be the time-dependent configuration of the organism *relative to itself*. The actual displacement relative to the grid is not present, but determined by the solution to the fluid equations.

As presented in [4], we use forces which are derived from a time dependent energy function $E_l(\mathbf{X}_{1,l}, \mathbf{X}_{2,l}, ..., \mathbf{X}_{m(l),l}, t)$ which is invariant under translation and rotation:

$$\mathbf{f}_{k,l} = -\partial_k E_l = -\left[\frac{\partial E_l}{\partial x_k}, \frac{\partial E_l}{\partial y_k}\right].$$

E_l is chosen so that $E_l \geqslant 0$ and $E_l = 0$ when the boundary configuration is as desired.

We want to control the arclength between successive points on an immersed boundary and the angle formed by the two "links" at each point:

$$E_l(\mathbf{X}_{1,l}, \mathbf{X}_{2,l}, \ldots, \mathbf{X}_{M,l}, t) = S_1 \sum_k \{\|\mathbf{X}^n_{k+1,l} - \mathbf{X}^n_{k,l}\| - \Delta s\}^2$$
$$+ S_2 \sum_k \{\tilde{z} \cdot (\mathbf{X}^n_{k+1,l} - \mathbf{X}^n_{k,l}) \times (\mathbf{X}^n_{k,l} - \mathbf{X}^n_{k-1,l}) - C_{k,l}(t)\}^2.$$

Here $\tilde{z} = (0, 0, 1)$. This is zero when the arclength is Δs and the "curvature" at the point $\mathbf{X}_{k,l}$ is $C_{k,l}(t)$. S_1 and S_2 are stiffness parameters which control how closely the configuration is enforced.

This energy function can be adjusted to enforce many different configurations by choosing an appropriate driving function $C_{k,l}(t)$. Note that this is where the time dependence of the swimming motion is established.

In this paper we will be considering sinusoidal motion of the form

$$y = b \sin(\kappa x - \omega t)$$

In this case

$$C_k(t) = -\kappa^2 b(\Delta s)^3 \sin(\kappa x - \omega t)$$
$$x = k\Delta s.$$

Once the force density is computed and spread to the grid to define $\mathbf{F}^n_{ij}$, the Navier–Stokes equations can be solved on a regular domain using simple boundary conditions. For this purpose we use Chorin's finite difference scheme [6] on a square, periodic grid. Once the fluid equations are solved, the velocity field is interpolated to the material points. These points are moved at the local fluid velocity. This completes one time step.

3. Interaction of Swimming Sheets

In his paper of 1951, G. I. Taylor analyzed the swimming motion of a doubly infinite sheet which undergoes periodic deformations about an unperturbed centerline $y = 0$. These deformations were taken to be very small compared to the wavelength of the sheet and of constant amplitude b. A two-dimensional slice of the sheet is of the form

$$y = b \sin(\kappa x - \omega t).$$

These coordinates are taken with respect to "axes which are fixed relative to the mean position of the particles of the sheet" [1]. This sine wave travels to the right with speed $V = \omega/\kappa$.

Using the linear Stokes equations to describe zero Reynolds number flow, Taylor calculated that the mean dissipation of energy (averaged over a period $2\pi/\omega$) on one side of the sheet is

$$E = b^2\omega^2\kappa\mu,$$

where μ is the viscosity of the fluid. This was calculated using an asymptotic expansion of the stream function and boundary conditions in powers of $b\kappa$ only up to $O(b\kappa)$. However, using this first-order expansion, it can be shown that the mean swimming speed of the sheet is zero. Up to the first order in the amplitude, the sheet does work, but it does not swim. When the asymptotic expansion is taken to second order in $b\kappa$, there is indeed swimming. A useful nondimensional parameter is the mean swimming speed U divided by the wavespeed $V = \omega/\kappa$. Using this higher order expansion, Taylor arrived at

$$\frac{U}{V} = \frac{1}{2}b^2\kappa^2\left(1 - \frac{19}{16}b^2\kappa^2 + O(b^6\kappa^6)\right),$$

where the direction of swimming is opposite to that of the wave.

In [4] we compared our calculations with Taylor's expressions for both energy dissipation and swimming speed in the case of a single doubly infinite sheet.

In this section, we study the interaction of more than one waving sheet immersed in the same domain of fluid. Each sheet is taken to have the same amplitude, wavelength, and frequency, but the phase difference is varied.

Consider two sheets whose centerlines are a distance of $2h$ apart:

$$y_1 = +h + b\sin(\kappa x - \omega t + \phi)$$
$$y_2 = -h + b\sin(\kappa x - \omega t - \phi).$$

Waves of the same amplitude travel down both sheets with the same speed, but the phase of the second lags behind that of the first by an angle 2ϕ.

In this case, Taylor assumes that the stream function is

$$\psi = (A_1 y\sinh\kappa y + B_1\cosh\kappa y)\cosh\phi\sin(\kappa x - \omega t)$$
$$+ (A_2\cosh\kappa y + B_2\sinh\kappa y)\sin\phi\cos(\kappa x - \omega t).$$

Boundary conditions are then imposed on the *centerlines* of the sheets:

$$\frac{\partial\psi}{\partial y} = 0 \qquad y = \pm h$$

$$\frac{\partial\psi}{\partial x} = \omega b\cos(\kappa x - \omega t + \phi) \qquad y = +h$$

$$\frac{\partial\psi}{\partial x} = -\omega b\cos(kx - \omega t - \phi) \qquad y = -h.$$

Using these conditions, the constants A_1, A_2, B_1, B_2 are obtained in terms of the parameters b, ω, κ, and h. The mean rate of dissipation of energy between the two sheets is calculated to be

$$E = \mu\kappa b^2\omega^2(\alpha \cos^2\phi + \beta \sin^2\phi),$$

where

$$\alpha = \frac{\sinh^2 \kappa h}{\sinh \kappa h \cosh \kappa h + \kappa h}, \qquad \beta = \frac{\cosh^2 \kappa h}{\sinh \kappa h \cosh \kappa h - \kappa h}.$$

This is also equal to the mean rate at which a unit length of the sheet does work on the fluid. The above expression achieves its minimum when $\phi = 0$ (sheets in phase) and its maximum when $\phi = \pi/2$ (sheets in opposite phase). The ratio of this maximum energy dissipation to minimum energy dissipation increases as the distance between the sheets decreases. Waving filaments close together require much less effort if they beat in unison as opposed to beating out of phase.

This asymptotic analysis is restricted to zero Reynolds number flow and small amplitude motion. The form of the stream function also does not allow for any propulsive motion. *Waving* sheets are being studied, not *swimming* sheets.

Our computational model solves the full Navier–Stokes equations, and therefore the effects of inertia can be considered. Also, we can study actual swimming of neighboring sheets, which the asymptotic method outlined above excludes. In this section we shall compare our results with the asymptotics for energy dissipation. We will show that certain phase differences are not stable—the swimming speeds of neighboring sheets differ. In the next section, we will present two case studies which show that these differing speeds provide a mechanism whereby sheets can alter their phase differences until a stable configuration is achieved.

Computational Studies

In order to stimulate the doubly infinite sheets, we impose periodic boundary conditions on our square computational domain. The length of one side of this domain is equal to one wavelength of the sine wave, $2\pi/\kappa$. The centerlines of the two filaments are placed one half of one wavelength apart. Each filament extends from one end of the domain to the other. We have *explicitly* linked the first and last point (modulo wavelength) of the immersed boundaries by coupling these points in the energy function. This simulates the infinite extent of the sheet. Additionally, because of the periodic boundary conditions in the vertical as well as horizontal direction, we are actually modelling an infinite array of equally spaced sheets of infinite extent. We stress that this technique can model more realistic organisms of finite extent, but we wish to compare our results with the asymptotics.

All of the computations presented in this paper were performed on the CRAY X-MP at the Pittsburgh Supercomputing Center. Figure 1 shows typical flow fields in the cases:

(1) $\phi = 0$ sheets in phase

(2) $\phi = \pi/4$ sheets 90° out of phase

(3) $\phi = \pi/2$ sheets in opposite phase.

In this particular case the wavelength was 0.2 cm, and the amplitude $b = 0.005$ cm. These are snapshots of the streamlines and positions of the boundaries. Because of the periodicity conditions, two domains are placed side by side. Notice that the fluid directions between the boundaries in the in-phase case are

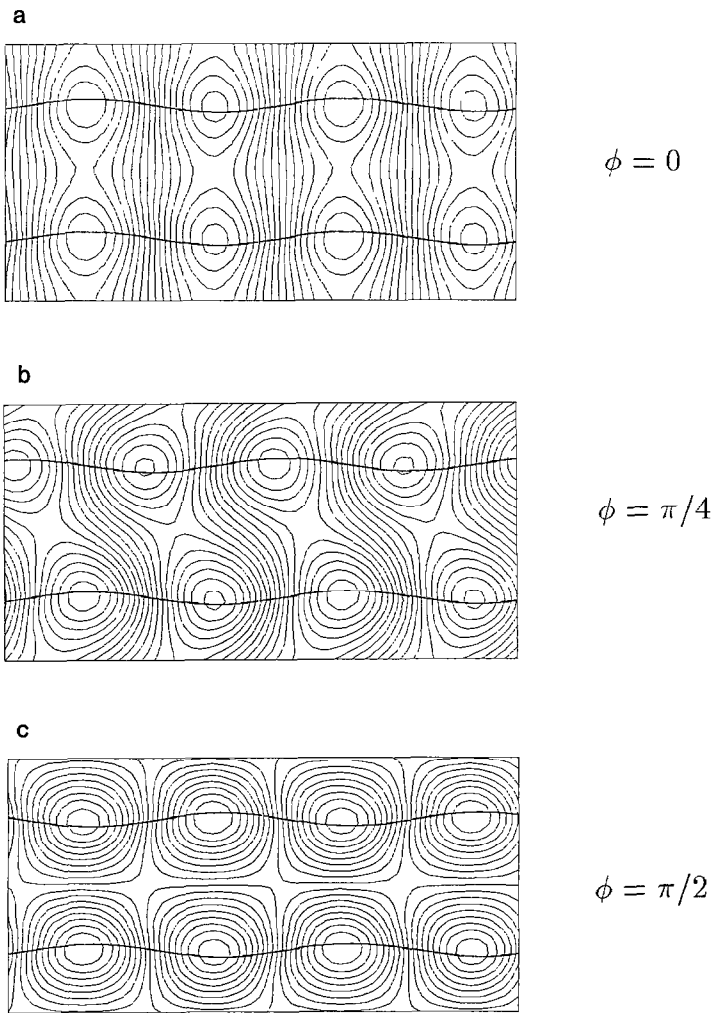

FIG. 1. Positions of filaments and streamlines of velocity field in the cases (a) $\phi = 0$, (b) $\phi = \pi/4$, (c) $\phi = \pi/2$. Dimensions of rectangle are 0.4 cm × 0.2 cm.

TABLE I

Phase Studies

Parameter	Symbol	Units	I	II	III
Wave number	κ	cm^{-1}	10π	10π	10π
Frequency	ω	s^{-1}	8π	8π	8π
Density	ρ	gm/cm^3	1	1	1
Amplitude	ε	cm	0.002	0.002	0.002
Viscosity	μ	gm/cm · s	0.01	0.05	0.05
Reynolds number	R	—	2.5	0.5	0.5
Proximity	2h	cm	0.1	0.1	0.05

mostly vertical, wheras in the opposite-phase case they are mostly horizontal. The latter case bears a striking resemblence to the flow fields induced by peristaltic pumping in two dimensions [7].

In the following phase studies I and II, the parameter values in Table I were fixed, but the initial phase difference between the two filaments was varied from $\phi = 0$ to $\phi = \pi/2$ in increments of $\pi/16$. We shall use a Reynolds number based upon wavelength,

$$R = \frac{\rho\omega}{\mu\kappa^2}.$$

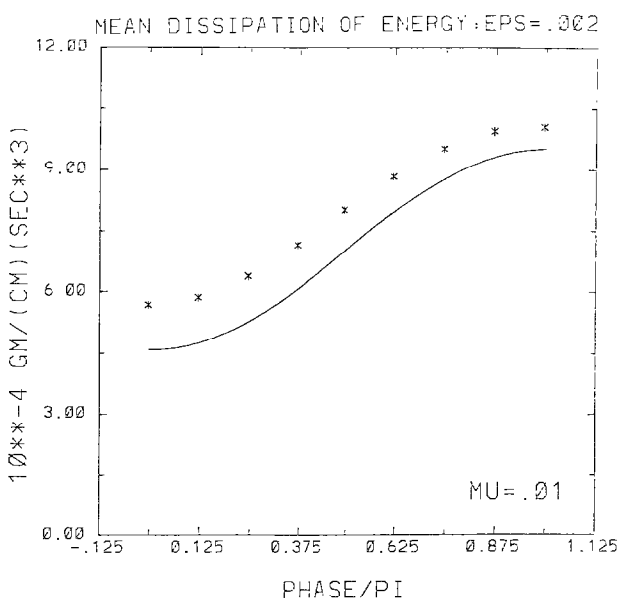

FIG. 2. Phase Study I. The mean dissipation of energy averaged over a period vs phase difference measure $2\phi/\pi$, $R \approx 2.5$.

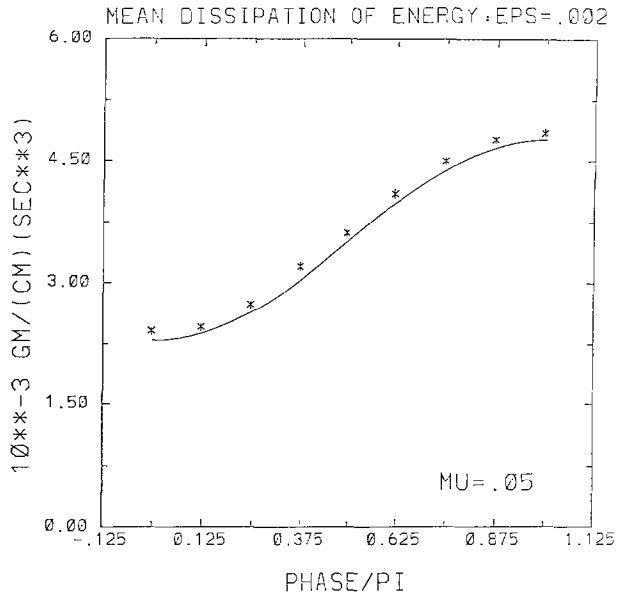

FIG. 3. Phase Study II. The mean dissipation of energy averaged over a period vs phase difference measure $2\phi/\pi$, $R \approx 0.5$.

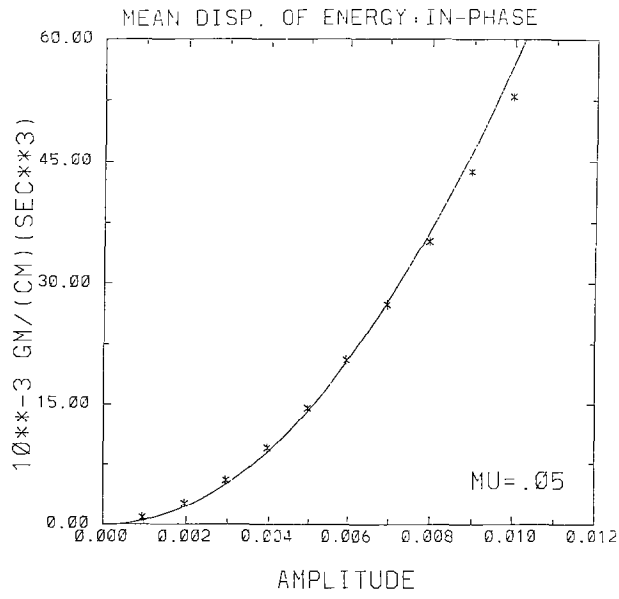

FIG. 4. The mean dissipation of energy averaged over a period vs amplitude. Here $\phi = 0$ and the other parameters are as in Phase Study II.

The calculations were performed on a 64×64 grid with 128 points comprising each immersed boundary. The velocity field was initialized to zero. In each numerical experiment, the code was run until an approximate (periodic) steady state was reached, which took at most four periods. By approximate steady state we mean that the average energy dissipation over a period was approximately equal to the average rate of working; the average rate of change of kinetic energy was small.

Figure 2 shows the total average energy dissipation in the fluid domain computed in phase study I ($R \approx 2.5$). The *'s indicate the computed values, and the solid curve indicates Taylor's asymptotic formula. For each phase difference the force is specified so that the same, constant amplitude oscillations of the sinusoidal filament are enforced. In each phase study this amplitude was $\varepsilon = 0.002$ cm, 1 % of a wavelength. Figure 3 shows the results from phase study II ($R \approx 0.5$). Note how much closer the asymptotic predictions are to the computed values in this much lower Reynolds number case. Also, the energy dissipation when the sheets are in opposite phase is about twice as much as when they are in phase.

Using the same parameter values as in phase study II, we fix the phase difference at zero, but vary the amplitude from 1 % of the wavelength, up to 5 % of the wavelength. The results of these computations are shown in Fig. 4. Note the excellent agreement with the asymptotics. For larger amplitudes, however, the discrepancy increases.

In both of the above studies, the array of sheets were equally spaced at one half of one wavelength apart. In phase study III ($R \approx 0.5$) we space the sheets at one quarter of one wavelength apart. The parameter values are given in Table I. In order to preserve symmetry and compare with the asymptotics, we put four immersed boundaries in the computational domain. Figure 5 shows a snapshot of the streamlines and boundaries in the opposite-phase case. Figure 6 shows the computed energy dissipation vs the asymptotics. Since Taylor's formula gives the energy dissipation between two sheets per unit length of one sheet, we must multiply the formula by 4×0.2 in order to calculate the total energy dissipation in

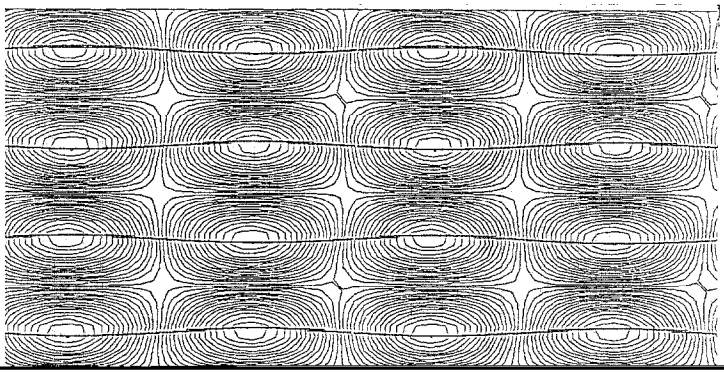

FIG. 5. Snapshot of streamlines and flowfields in the opposite-phase case. Here there are four immersed boundaries per computational domain.

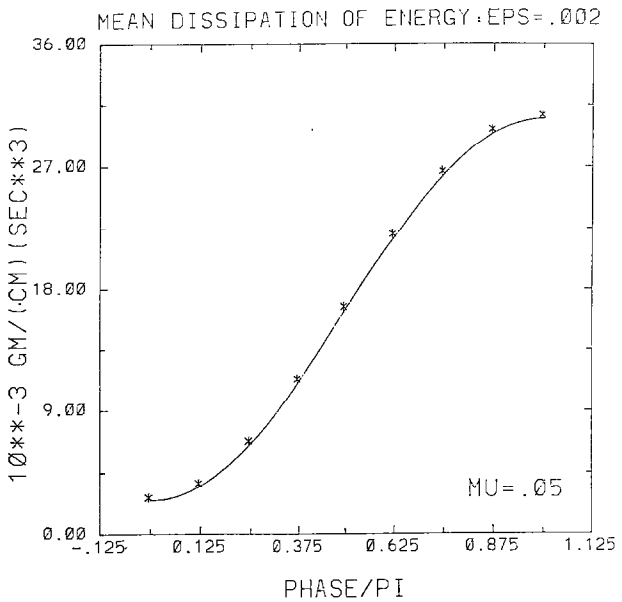

FIG. 6. Phase Study III. The mean dissipation of energy averaged over a period vs phase difference measure $2\phi/\pi$, $R \approx .5$.

the domain. Here, the energy dissipation in the opposite-phase case is about twelve times that of the in-phase case.

Thus far, we have only indicated the computed energy dissipation but have not commented on the swimming progress. In phase study I, when the sheets start out oscillating in phase, the mean swimming velocities over a period were the same: $U_1 = U_2 = 8.95 \times 10^{-4}$ cm/s. When the sheets were oscillating in opposite phase, again they swam at the same velocity as each other, but this time $U_1 = U_2 = 2.52 \times 10^{-3}$ cm/s. This is a reasonable result, since in the second instance, the region

TABLE II

Mean Swimming Velocities in 10^{-3} cm/s Phase Study I

ϕ	U_1	U_2
0	0.895	0.895
$\pi/16$	0.502	1.43
$\pi/8$	0.312	2.00
$3\pi/16$	0.349	2.52
$\pi/4$	0.599	2.90
$5\pi/16$	1.01	3.10
$3\pi/8$	1.52	3.09
$7\pi/16$	2.04	2.89
$\pi/2$	2.52	2.52

of fluid between the boundaries is being pushed in the same direction; the sheets are helping each other swim.

In the other cases in phase study I, $\phi = l\pi/16$, $l = 1, 2, 3, ..., 7$, the sheets have different mean velocities. This is shown in Table II. This suggests that these phase differences give rise to unsteady configurations. One can expect that the velocities will adjust the relative positioning of the filaments until they are either in phase or in opposite phase, where the swimming speeds of the two filaments are equal. We conjecture that, depending upon the Reynolds number and the proximity of the sheets, one of these steady configurations will be stable and the other unstable. We will present case studies in the next section which support this conjecture.

4. Case Studies

Again, we consider an infinite array of equally spaced doubly infinite waving sheets, where each sheet oscillates with the same amplitude, wavelength, and frequency, but there is a phase-shift between neighboring sheets. We have evidence that when the phase-shift $\tilde{\phi} = 2\phi$ is 0 (in-phase) or $\tilde{\phi} = 2\phi$ is π (opposite-phase) the mean swimming speed of each sheet is the same, and thus the phase-shifts remain at $\tilde{\phi} = 0$ or $\tilde{\phi} = \pi$, respectively. However, intermediate phase differences $0 < \tilde{\phi} < \pi$ lead to unsteady configurations. This is manifested in differing mean velocities of neighboring sheets. For instance, refer back to Fig. 1. The first and third flowfields corresponding to $\tilde{\phi} = 0$ and $\tilde{\phi} = \pi$ are in equilibrium. We expect that one of these equilibria will be stable and the other unstable. The second flowfield, where $\tilde{\phi} = \pi/2$, is an unsteady configuration. If the top filament were to "swim slower" than the bottom filament to the left, then at some point they would be in phase. If the top filament were to "swim faster," at some point they would be in opposite phase. The occurrence of "phase-locking" or "opposite phase-locking" will be explored in the following two case studies.

Case Study 1

The following numerical experiment used a 64×64 square grid, with four immersed boundaries of 128 points each. Periodic boundary conditions simulate an infinite array of waving filaments spaced equally at one quarter of one wavelength apart. The physical parameters and numerical parameters used are presented in Table III. The phase speed of the sine wave is 0.8 cm/s, and the period of motion is 0.25 s. We initialized the velocity field to zero and the initial phase-shift to $\tilde{\phi} = \pi/2$. The Reynolds number in this case is quite small, approximately 0.25.

In order to study how the velocities will alter the phase differences in the long run, we ran the code for 32,000 time steps, 160 periods, up to $t = 40$ s. (This took about 12 h of CRAY time.) Figure 7 shows snapshots of the filaments and the flowfields at intervals of 4 s, from $t = 4$ through $t = 40$ s. The filaments have phase-locked! Figure 8 shows the mean dissipation of energy averaged over each of the 160 periods. The energy is monotonically decreasing as the phase difference of the

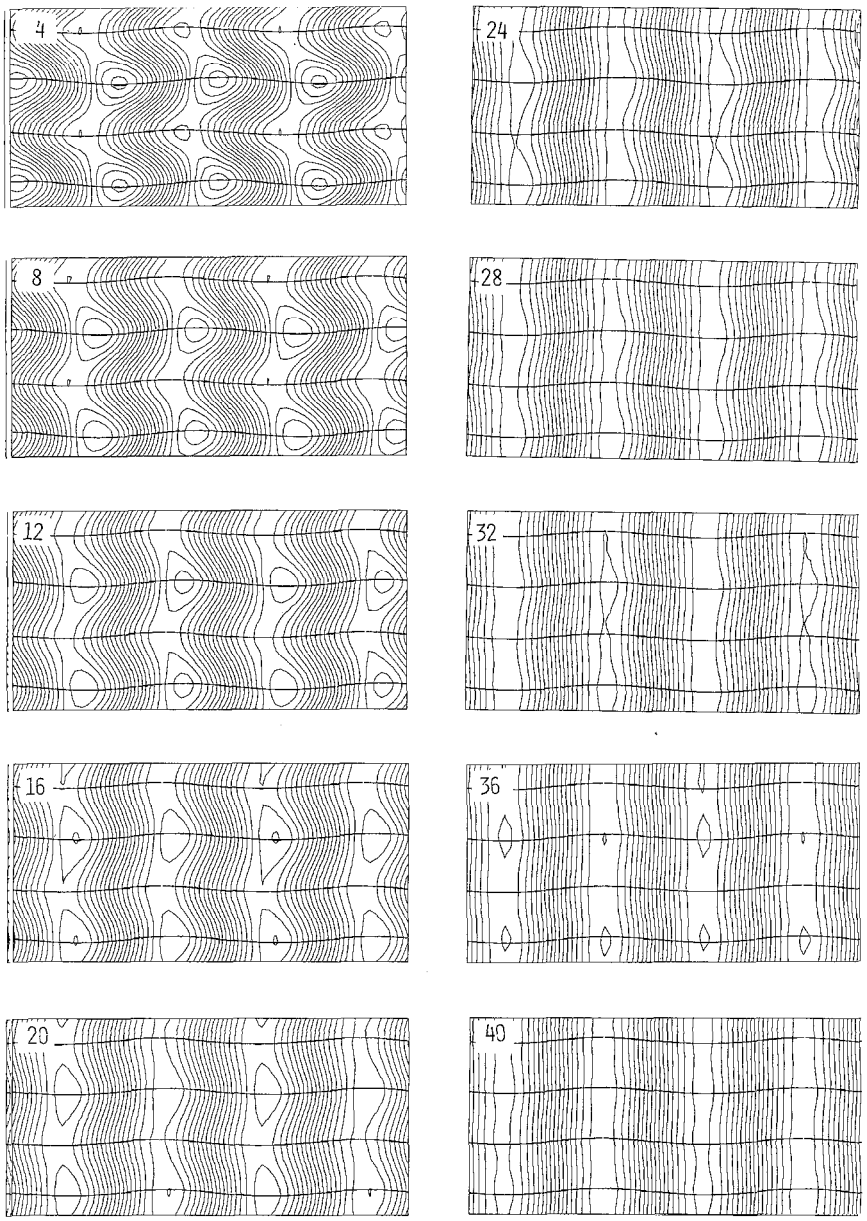

FIG. 7. Snapshots of the filaments and the flowfields in Case Study 1 at intervals of four second, from $t = 4$ through $t = 40$ s.

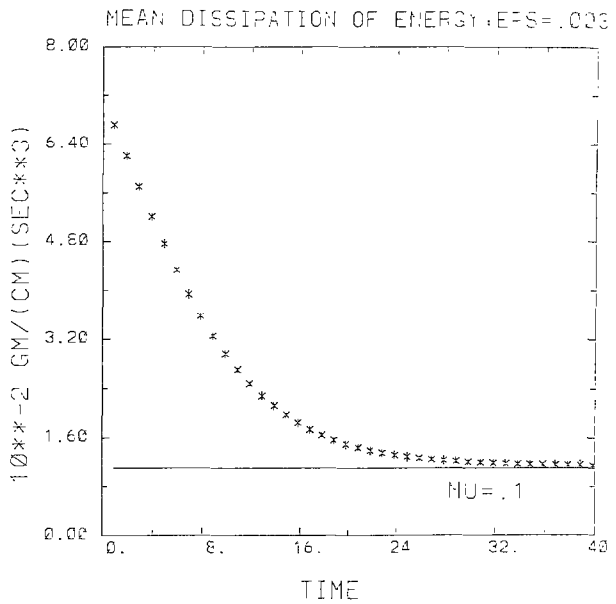

FIG. 8. Case Study 1. Mean average dissipation of energy vs period (1 period = 0.25 s. EPS = 0.003).

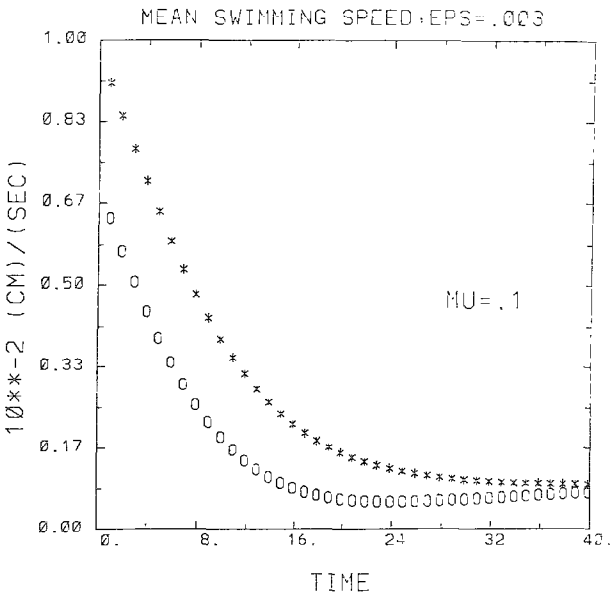

FIG. 9. Case Study 1. Mean swimming speeds of the filaments vs period. The upper curve (*'s) corresponds to the bottom most filament in the domain, the lower curve (O's) to the neighboring filament. The other two filaments have corresponding velocities due to symmetry. EPS = 0.03.

filaments goes from $\tilde{\phi} = \pi/2$ down to $\tilde{\phi} = 0$, leveling off at Taylor's predicted value of in-phase energy dissipation (the horizontal line). Figure 9 shows the mean swimming speeds of the two filaments at each period. The upper curve corresponds to the bottommost filament in the domain, and the lower curve corresponds to the neighboring filament. The speeds of the other two filaments are the same due to symmetry. One cannot note the progress in the direction of swimming in Fig. 7 due to the periodicity of the filaments. However, the mean velocities are calculated using the positions of the *material* points of the filaments. The velocities of each filament decrease as they tend to phase-lock.

The mechanism whereby the phase difference between neighboring sheets $\tilde{\phi}$ changes is the differing velocities of the sheets. These velocities themselves depend on the phase difference

$$v_1 = f_1(\tilde{\phi})$$

$$v_2 = f_2(\tilde{\phi})$$

Let D be the horizontal distance between the crests on neighboring filaments. We have

$$\tilde{\phi} = 2\pi \frac{D}{\lambda},$$

where λ is the wavelength of each sheet and

$$\frac{dD}{dt} = v_1 - v_2.$$

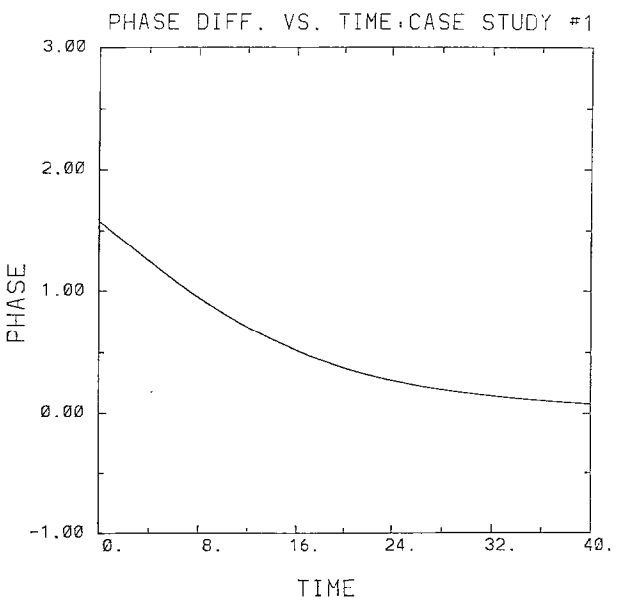

FIG. 10. Case Study 1. The phase difference vs time arrived at by solving the ordinary differential equation for ϕ.

Therefore,

$$\frac{d\bar{\phi}}{dt} = \frac{2\pi}{\lambda}\left[f_1(\bar{\phi}) - f_2(\bar{\phi})\right].$$

Given the functions $f_1(\bar{\phi})$ and $f_2(\bar{\phi})$, we would integrate this ordinary differential equation and determine the evolution of $\bar{\phi}$. We do not know the explicit form of these functions, but we can tabulate their values at different values of $\bar{\phi}$.

The code was run with the same parameter values as in Case Study 1, but with the initial phase difference $\bar{\phi}$ varying from 0 to π in increments of $\pi/8$, for only four periods. The velocities are small enough so that the phase differences barely change from their initial values during this short time span. These short runs enable us to tabulate the functions $f_1(\bar{\phi})$ and $f_2(\bar{\phi})$ for $\bar{\phi} = l\pi/8$, $l = 0, 1, 2, \ldots, 7, 8$. The functions at intermediate values can be interpolated from these.

We discretize the initial value problem

$$\bar{\phi}(t + \Delta t) = \bar{\phi}(t) + \Delta t \frac{2\pi}{\lambda}\left(f_1(\bar{\phi}(t)) - f(\bar{\phi}(t))\right)$$

$$\bar{\phi}(0) = \pi/2,$$

where $\Delta t = 0.125$ s.

The solution of this differential equation is shown in Fig. 10. We see again that the filaments have phase-locked.

In this case study, the motion has evolved into one which minimizes the expended energy. One is tempted to conjecture that this should always be the case. As our next case study will show, this is not true.

Case Study 2

The set-up of this numerical experiment is the same as the foregoing except that now we have only two immersed boundaries in the domain. This simulates an

TABLE III

Case Studies

Parameter	Symbol	Units	I	II
Wave number	κ	cm^{-1}	10π	10π
Frequency	ω	s^{-1}	8π	8π
Density	ρ	gm/cm^3	1	1
Amplitude	b	cm	0.003	0.002
Viscosity	μ	gm/cm · s	0.1	0.01
Reynolds number	R	—	0.25	2.5
Proximity	$2h$	cm	0.05	0.1
Grid spacing	Δx	cm	0.003125	0.003125
Time step	Δt	s	0.00125	0.00125
Arclength	Δs	cm	$0.5\Delta x$	$0.5\Delta x$
Stiffness S_1	S_1	—	$10{,}000(\Delta s)^{-1}$	$10{,}000(\Delta s)^{-1}$
Stiffness S_2	S_2	—	$10(\Delta s)^{-5}$	$10(\Delta s)^{-5}$

infinite array of sheets spaced one half of one wavelength apart. The parameters used are also presented in Table III. Here the Reynolds number is ten times larger than Case Study 1, and the sheets are spaced at twice the distance.

We ran the code for 48,000 time steps. 240 periods, up to $t = 60$ s. (This took considerably less CRAY time, since we only had two immersed boundaries per domain.) Figure 11 shows snapshots of the filaments and the flowfields at intervals of 4 s, from $t = 4$ through $t = 60$ s. Here, the filaments have "opposite" phase-locked! Figure 12 shows the mean dissipation of energy averaged over each of the 240 periods. Now the energy is monotonically increasing until it levels off. Figure 13 shows the mean swimming velocities at each of the periods. The upper curve corresponds to the top filament and the lower curve to the bottom filament in the

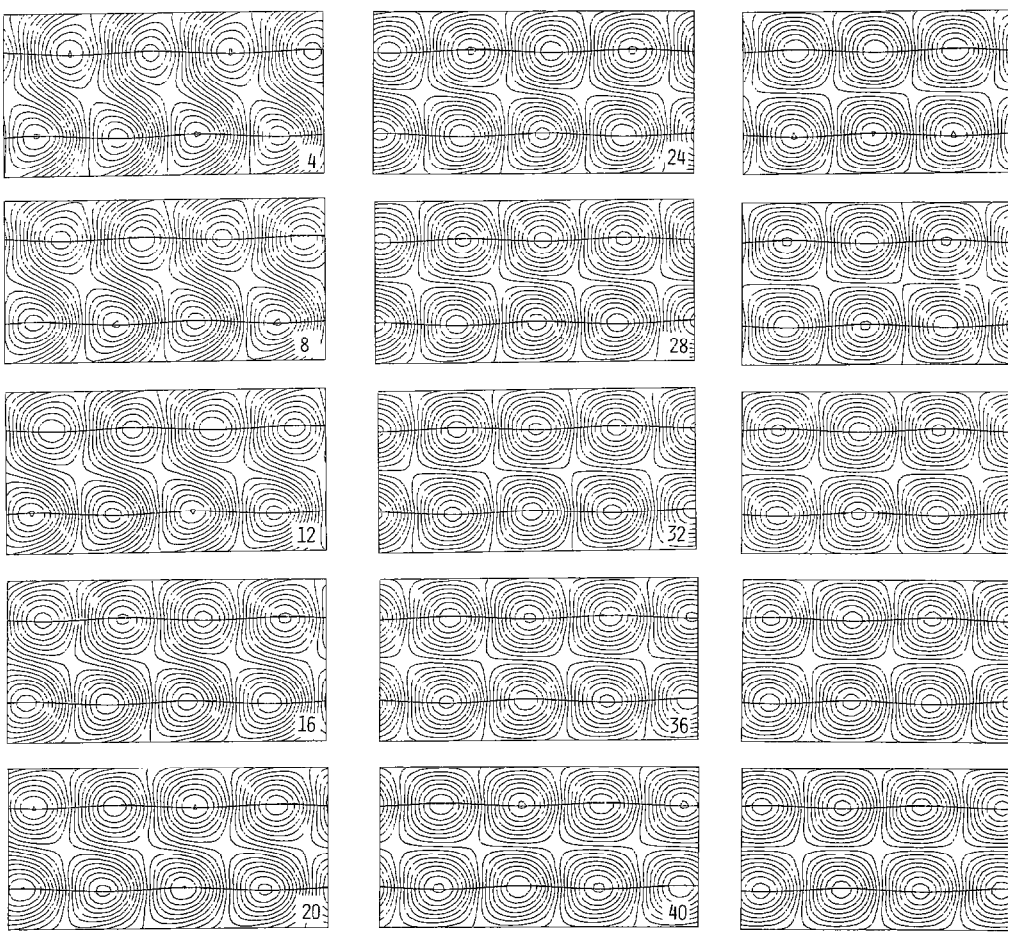

FIG. 11. Snapshots of the filaments and the flowfields in Case Study 2 at intervals of four seconds from $t = 4$ throught $t = 60$ s.

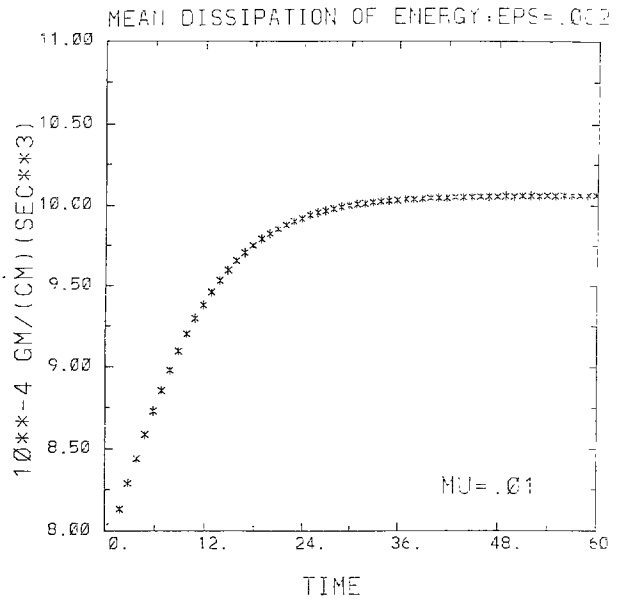

FIG. 12. Case Study 2. Mean average dissipation of energy vs period (1 period = 0.25 s, EPS = 0.002).

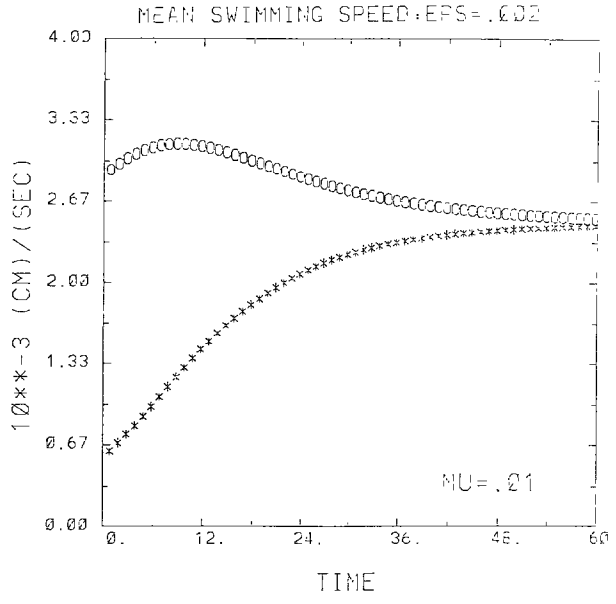

FIG. 13. Case Study 2. Mean swimming speeds of the filaments vs period. The upper curve (o's) corresponds to the top filament and the lower curve (*'s) to the bottom filament. EPS = 0.002.

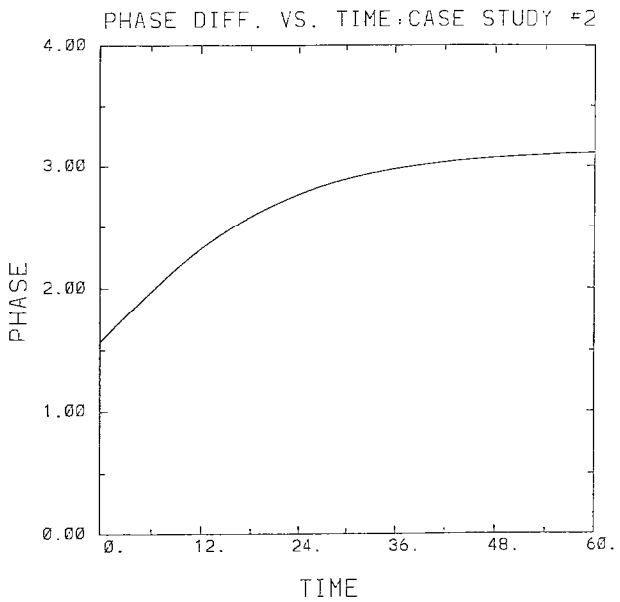

FIG. 14. Case Study 2. The phase difference vs time arrived at by solving the ordinary differential equation for ϕ.

domain. In this case study, the energy dissipation is not minimized as before, but the average swimming speeds of the sheets is maximized.

Again, we also use the ordinary differential equation to analyze the change in the phase difference of neighboring filaments in Case Study 2. The results are shown in Fig. 14.

5. CONCLUSIONS

In this paper we applied the immersed boundary technique to computationally model the interaction of oscillating filaments in an incompressible, viscous fluid. We have evidence which suggests that, indeed, the least amount of energy is dissipated when the filaments wave in-phase, as G. I. Taylor showed for zero Reynolds number, small amplitude motion. However, we also have evidence that the mean swimming velocities are maximized when the filaments are in opposite phase.

We conjecture that the in-phase case and opposite-phase case are equilibria, and that one of these is stable and the other unstable—depending upon the Reynolds number and the proximity of the filaments. We would like to know what this dependence is. The question of phase-locking or "opposite" phase-locking of an array of oscillating filaments, to our knowledge has not been addressed analytically. Using the immersed boundary technique, we are able to follow the evolution of this nonlinear dynamical system for fixed parameter values. Together with the ordinary

differential equation formula of the change in phase difference, we have an economical algorithm which tests for phase-locking or "opposite" phase-locking. We propose to do further tests to determine what the conditions on the parameters are in either case.

REFERENCES

1. G. I. TAYLOR, *Proc. Roy. Soc. Ser. A* **209**, 447 (1951).
2. D. WEIHS, *Nature* **241**, 290 (1973).
3. M. A. SLEIGH AND D. I. BARLOW, "Metachronism and Locomotion," *Aspects of Animal Movement*, edited by Elder and Trueman (Cambridge Univ. Press, Cambridge, 1980), p. 49.
4. L. J. FAUCI AND C. S. PESKIN, *J. Comput. Phys.* **77**, 85 (1988).
5. C. S. PESKIN, *J. Comput. Phys.* **25**, 220 (1977).
6. A. J. CHORIN, *Math. Comput.* **22**, 745 (1968).
7. BURNS AND PARKES, *J. Fluid Mech.* **29**, 731 (1967).
8. LIGHTHILL, *Mathematical Biofluidmechanics*, Regional Conference Series in Applied Mathematics, Vol. 17 (SIAM, Philadelphia, 1975).